Annals of Biomedical Engineering (© 2022)
https://doi.org/10.1007/s10439-022-03093-x

BMES BIOMEDICAL ENGINEERING SOCIETY

Original Article

Pentagalloyl Glucose (PGG) Prevents and Restores Mechanical Changes Caused by Elastic Fiber Fragmentation in the Mouse Ascending Aorta

Christie L. Crandall,[1] Bryant Caballero,[1] Mariana E. Viso,[1] Naren R. Vyavahare,[2] and Jessica E. Wagenseil[1]

[1]Department of Mechanical Engineering and Materials Science, Washington University, St. Louis, MO, USA; and [2]Department of Bioengineering, Clemson University, Clemson, SC, USA

(*Received 23 June 2022; accepted 28 September 2022*)

Associate Editor Stefan M. Duma oversaw the review of this article.

Abstract—Thoracic aortic aneurysm (TAA) is characterized by dilation of the aorta that can lead to dissection or rupture. Degradation of elastic fibers is a consistent histopathological feature of TAA that likely contributes to disease progression. Pentagalloyl glucose (PGG) shows promise for stabilizing elastic fibers in abdominal aortic aneurysms, but its efficacy and mechanical effects in the thoracic aorta are unknown. We simulated TAAs using elastase (ELA) to degrade elastic fibers in the mouse ascending aorta and determined the preventative and restorative potential of PGG. Biaxial mechanical tests, constitutive model fitting, and multiphoton imaging were performed on untreated (UNT), PGG, ELA, PGG + ELA, and ELA + PGG treated aortas. PGG treatment alone does not significantly alter mechanical properties or wall structure compared to UNT. ELA treatment alone causes an increase in the unloaded diameter and length, decreased compliance, significant changes in the material constants, and separation of the outer layers of the aortic wall compared to UNT. PGG treatment before or after ELA ameliorates the mechanical and structural changes associated with elastic fiber degradation, with preventative PGG treatment being most effective. These results suggest that PGG is a potential pharmaceutical option to stabilize elastic fibers in TAA.

Keywords—Thoracic aortic aneurysm, Elastase, Elastin, Biomechanics.

ABBREVIATIONS

AAA	Abdominal aortic aneurysm
ATA	Ascending thoracic aorta
ELA	Elastase
HGO	Holzapfel–Gasser–Ogden
PBS	Phosphate buffered saline
PGG	Pentagalloyl glucose
TAA	Thoracic aortic aneurysm
UNT	Untreated

Address correspondence to Jessica E. Wagenseil, Department of Mechanical Engineering and Materials Science, Washington University, St. Louis, MO, USA. Electronic mail: jessica.wagenseil@wustl.edu

INTRODUCTION

Thoracic aortic aneurysms (TAA) are a prominent health concern affecting 5.3 per 100,000 people/year and are considered "silent killers" due to their asymptomatic nature.[6] Early diagnosis and intervention are crucial to prevent TAA dissection or rupture and adverse outcomes for TAA patients.[20] A main contributor to TAA are defects in the extracellular matrix, specifically, the elastic fibers. This is evidenced by TAA-linked genetic mutations that affect pathways involved in elastic fiber formation and crosslinking.[12,24] Improperly assembled elastic fibers may be more susceptible to degradation and contribute to aneurysm progression over time.[7] Elastic fiber fragmentation is a common histopathological finding in TAA, regardless of the underlying cause.[20] Elastic fibers are essential to the aorta because of their elastic material properties that allow the artery to respond to large, cyclic pressure and volume changes.[33] Standard TAA treatment includes regular imaging followed by surgical replacement when the size or growth rate of the aortic diameter exceeds specified thresholds.[20] Due

Published online: 06 October 2022

to the complications that can arise with surgery, there is a need for pharmaceutical therapies that could prevent or counter the effects of extracellular matrix degradation, aortic wall dilation, and eventual dissection or rupture.

Pentagalloyl glucose (PGG) is the non-cytotoxic core structure of tannic acid, which is a naturally occurring plant polyphenol. PGG binds to elastin, stabilizes arterial elastic fibers, and prevents degradation by the enzyme elastase (ELA).[21] PGG has been used *in vivo* in mouse, rat, and pig models to stabilize elastic fibers and prevent dilation of chemically-induced abdominal aortic aneurysms (AAAs).[9,28,32,35] PGG has beneficial effects on other pathways involved in AAA progression, including reduced matrix metalloproteinase production, macrophage infiltration, and/or TGF-β1 activity.[9,22,35] Elastic fiber degradation contributes to mechanical changes in the aortic wall and releases elastin derived peptides that can exacerbate these pathological pathways and contribute to cardiovascular disease.[11] Hence, focusing on PGG's effects on preventing elastic fiber degradation and mechanical changes in the aortic wall are reasonable starting points for evaluating its utility in aneurysm treatment. The mechanical restorative potential of PGG was quantified through biaxial mechanical testing of pig abdominal aorta after ELA treatment.[29] While the data on PGG in AAA models is promising, there are known differences in AAA and TAA arterial wall structure, disease causes, disease progression, and clinical outcomes, necessitating investigation of PGG's potential for stabilizing elastic fibers in the thoracic aorta.

Previously, we quantified the mechanical preventative potential of PGG through pressure-diameter testing of mouse carotid arteries after ELA treatment.[30] We did not investigate the mechanical restorative potential of PGG or its effects on biaxial mechanical behavior, which are both important for clinical applications. There are significant differences in the size, elastin content, and aneurysm susceptibility between carotid arteries and the thoracic aorta that motivate studies on the arterial segment of interest. Additionally, previous *in vitro* studies with PGG delivered the drug directly to the inner and outer arterial surface by submersion of the tissue.[29,30] For clinical treatment, PGG would likely be delivered intravenously to contact the inner aortic surface only and this delivery method should be replicated if possible when determining PGG efficacy in stabilizing elastic fibers.

Here, we investigate the preventative and restorative mechanical potential of PGG in the mouse ascending aorta before or after treatment with ELA. We delivered all drugs (ELA and PGG) through the aortic lumen to better mimic clinical treatment methods. We optimized the ELA treatment timing to provide mild elastic fiber fragmentation and aortic dilation, as observed in TAA. We performed biaxial mechanical testing for each aorta in the untreated (UNT) and treated (PGG, ELA, PGG + ELA, ELA + PGG) state and fit a Holzapfel–Gasser–Ogden (HGO)[18] constitutive model to compare material properties and extrapolate results to common loading conditions. We used multiphoton imaging to identify changes in the extracellular matrix structure in response to the different treatments that may explain the mechanical changes. Our work helps to gain insight into the efficacy of PGG as a preventative and/or restorative treatment for TAA through stabilization of elastic fibers.

MATERIALS AND METHODS

Mice and Aortic Treatment Groups

C57BL6/J male mice (000664, Jackson Labs) ages 3–4 months were euthanized by carbon dioxide inhalation in compliance with the Institutional Animal Care and Use Committee (N = 36 total). Male mice were used to control for aortic size and mechanical behavior, which varies by sex.[17] Ascending thoracic aortas (ATAs) were isolated by dissection and kept in phosphate buffered saline (PBS) at 2–8 °C for up to four days before experimentation.[1] A pressure myograph and its accompanying software were used for biaxial mechanical testing and data acquisition (110P, Danish Myotechnology). ATAs were placed in a PBS bath at 37 °C and secured onto the myograph cannulae using 7–0 sutures. Each ATA served as its own untreated (UNT) control (N = 21) and was subjected to the mechanical test protocol described in the next section. After UNT data were collected, the ATA was treated with PGG (Sigma, #G7548), ELA (EPC, #EC134GI) or both drugs in sequential order (ELA + PGG or PGG + ELA) (Fig. 1) (N = 5–6/group). Each drug was injected into the ATA lumen and maintained in the lumen while the ATA was stretched axially and pressurized to 100 mmHg to mimic *in vivo* conditions and facilitate transmural drug transport.[16] After treatment, the aortic lumen was rinsed well with PBS and the mechanical test protocol was repeated again. ELA was used at 7.5 U/mL in PBS, held in the lumen for 6 min, and followed by 100 mM NaCl for 6 min to stop the enzymatic activity.[36] PGG was dissolved in DMSO, diluted to 0.37% w/w in PBS,[22] and held in the lumen for 7 min. ELA treatment dose and time were optimized in preliminary experiments to result in mild elastic fiber degradation and diameter dilation in the mouse ATA. PGG treat-

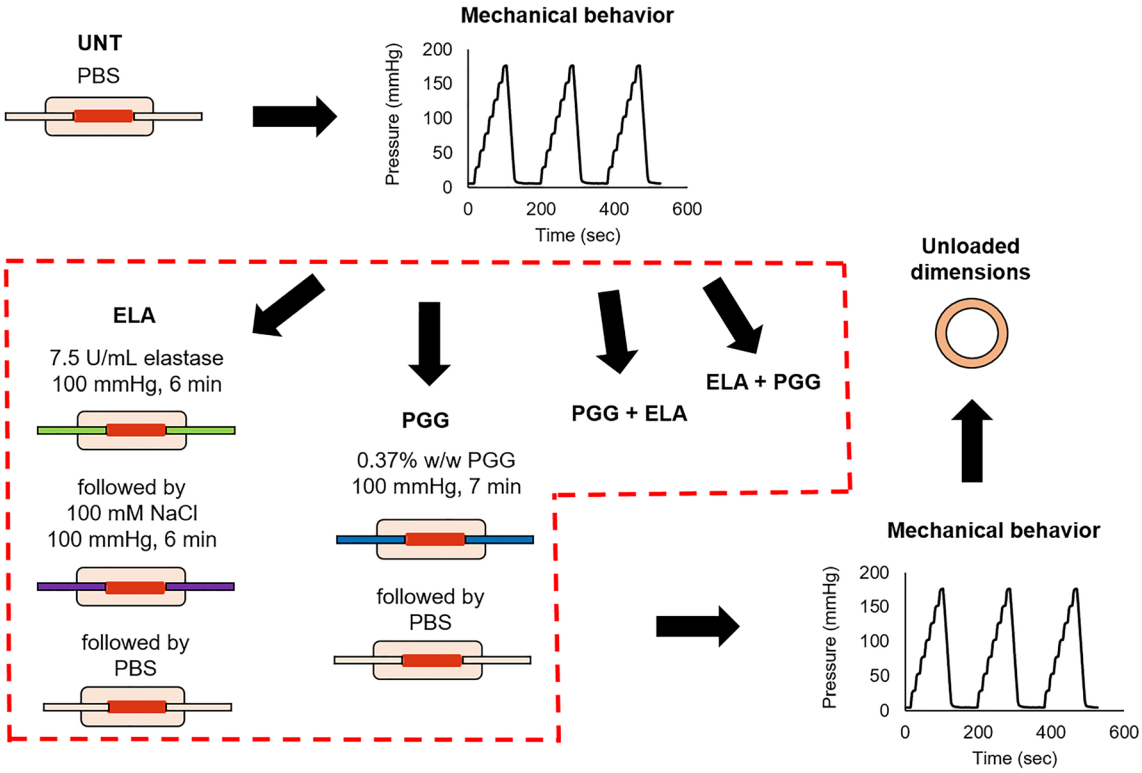

FIGURE 1. Experimental design demonstrating treatment groups and measurements. Each ATA served as its own untreated control (UNT) and was mechanically tested. ATAs were then placed into one of four treatment groups: ELA, PGG, PGG + ELA, or PGG + ELA. Post treatment, ATAs were mechanically tested again, then rings were cut to measure unloaded dimensions.

ment time was set to be approximately equal to ELA treatment time and is sufficient for a solute of PGG's size to transport through the wall of a mouse carotid artery pressurized at 100 mmHg.[8] Additional ATAs (N = 15 total, 3/group) underwent similar drug treatment protocols, but were then fixed at 100 mmHg for imaging rather than mechanically tested.

Biaxial Mechanical Testing

After preconditioning, ATAs underwent six mechanical testing protocols: three inflation cycles from 0 to 175 mmHg in increments of 25 mmHg for 12 s/step at three different constant axial stretch ratios and three axial stretch cycles at approximately 20 μm/s at three different constant pressures of 50, 100, and 150 mmHg, as done previously.[25] The lumen pressure (P), loaded outer diameter (do), and axial force (f) were recorded. The axial stretch ratios were calculated by noting the axial micrometer position at the beginning and end of the test protocol and assuming a constant stretch rate. The axial stretch ratio range varied by treatment group as we were not able to stretch any of the groups treated with ELA as far as the UNT group without tearing the tissue The axial stretch ratio ranges were approximately 1.4–1.8 for UNT and PGG and 1.0–1.2 for ELA, PGG + ELA, ELA + PGG groups. Each ATA underwent UNT mechanical testing, was treated, and then tested again. For all of the groups treated with ELA, a new unloaded length was determined before the post-treatment mechanical testing. After testing, the ATAs were removed from the myograph and 200–300 μm thick rings were cut and imaged (Fig. 1). Using ImageJ (NIH), the outer and inner boundaries of three rings/ATA were traced and ellipses were fit to determine the average unloaded outer (Do) and inner (Di) diameters. Due to the sequential nature of the treatment protocols, we did not have rings to determine the unloaded diameters for the UNT group. Subsequent analyses showed no significant differences in the unloaded dimensions of the PGG, PGG + ELA, and ELA + PGG groups, so the average unloaded dimensions from all ATAs in these three groups were used as the unloaded dimensions for the UNT ATAs.

Mechanical Data Analysis

From the data collected, the third loading cycle was used for analysis. Compliance was calculated from the average change in diameter per 25 mmHg pressure

step.[19] The stretch ratios (λ) in each direction (θ = circumferential, z = axial, and r = radial),

$$\lambda_\theta = \frac{1}{2}\left(\frac{d_i}{D_i} + \frac{d_o}{D_o}\right), \lambda_z = \frac{l}{L}, \lambda_r = \frac{1}{\lambda_\theta \lambda_z} \tag{1}$$

where d_i was calculated from the deformed and undeformed dimensions by conservation of volume, and the mean stresses (σ) in the circumferential and axial directions were determined assuming an incompressible cylinder with no shear,

$$\sigma_\theta = \frac{Pd_i}{d_o - d_i}, \sigma_z = \frac{4f + Pd_i^2}{\pi\left(d_o^2 - d_i^2\right)}. \tag{2}$$

The circumferential stretch vs. stress data were fit to an exponential equation,

$$\sigma_\theta = b_1 + b_2 \exp\left(\frac{\lambda_\theta^{b_3}}{b_4}\right), \tag{3}$$

where b_i are constants determined by regression using Matlab (Mathworks), that was differentiated to determine the circumferential tangent modulus (E_p),

$$E_p = \frac{d\sigma_\theta}{d\lambda_\theta}. \tag{4}$$

Constitutive Modeling

The data were fit to a HGO constitutive model that represents the passive strain energy function (W) for the aortic wall as a fiber-reinforced composite with an isotropic term (I) and an anisotropic term (A),[18]

$$W = W^I + W^A. \tag{5}$$

The isotropic term describes a neo-Hookean solid,

$$W^I = \frac{c_1}{2}(I_1 - 3), \tag{6}$$

where c_1 is a material parameter and the first invariant is $I_1 = \lambda_\theta^2 + \lambda_z^2 + \lambda_r^2$. The anisotropic term describes two symmetrically oriented fiber-families with exponential behavior,

$$W^A = \sum_{k=1}^{2} \frac{c_2}{2c_3}\left(e^{c_3\left(I_4^k - 1\right)^2} - 1\right), \tag{7}$$

where c_2 and c_3 are material parameters and the fourth invariant is $I_4^k = \lambda_\theta^2 \cos^2\left(\alpha^k\right) + \lambda_z^2 \sin^2\left(\alpha^k\right)$, where $\alpha^1 = +\alpha; \alpha^2 = -\alpha$ and α is the angle of the fiber families in the unloaded configuration with respect to the circumferential direction.

For an incompressible cylinder, the principle stresses can be calculated as,

$$\sigma_{ii} = 2F_{ii}^2 \frac{\partial W}{\partial C_{ii}} - p, \text{(not summed)} \tag{8}$$

where i = θ, r, or z, p is the Lagrange multiplier, the deformation gradient is $[\boldsymbol{F}] = \mathrm{diag}[\lambda_\theta, \lambda_z, \lambda_r]$, and the right Cauchy–Green strain tensor is $[\boldsymbol{C}] = diag\left[\lambda_\theta^2, \lambda_z^2, \lambda_r^2\right]$. Inflation and extension in the absence of shear requires $\sigma_{r\theta} = \sigma_{rz} = \sigma_{\theta z} = 0$.

The material parameters (c_1–c_3) and unloaded fiber family angle (α) were determined by constrained nonlinear regression to minimize the error between the experimental (Eq. 2) and predicted (Eq. 8) circumferential and axial stress values for every data point, i, using the *fmincon* function in Matlab. The error is defined as:

$$\text{Error} = \sqrt{\frac{\sum\left(\sigma_{\theta\theta,\exp}(i) - \sigma_{\theta\theta,\text{pred}}(i)\right)^2}{\sum\left(\sigma_{\theta\theta,\exp}(i)\right)^2}} + \sqrt{\frac{\sum\left(\sigma_{zz,\exp}(i) - \sigma_{zz,\text{pred}}(i)\right)^2}{\sum\left(\sigma_{zz,\exp}(i)\right)^2}}. \tag{9}$$

The material parameters were constrained to the positive domain, and α was only allowed to vary between 0° and 90° with 0° aligning with the circumferential axis. Parameter fitting was performed for each individual ATA with12 initial starting guesses distributed across the parameter space and using nonparametric bootstrapping for 2000 replicates (24,000 runs/ATA).[14] This resulted either in a set of parameters tightly distributed around a high R^2 or mostly distributed around a high R^2 with some cases where *fmincon* was satisfied at a lower R^2. We isolated only the fitted values distributed around the high R^2 and calculated the mean of the fitted parameters and R^2 for each ATA. We used these mean values as the optimized parameters for each ATA.

Representative fitted parameters from a single ATA in each group were used to determine representative strain energy, stresses, and linearized moduli under equivalent loading conditions. The linearized moduli (ζ) in the circumferential and axial directions were calculated by[3]:

$$\zeta_\theta = 4\lambda_\theta^2 \frac{\partial W}{\partial C_{\theta\theta}} + 4\lambda_\theta^4 \frac{\partial^2 W}{\partial C_{\theta\theta}^2}, \zeta_z = 4\lambda_z^2 \frac{\partial W}{\partial C_{zz}} + 4\lambda_z^4 \frac{\partial^2 W}{\partial C_{zz}^2}. \tag{10}$$

Imaging

For imaging, three ATAs underwent the standard drug treatment protocol for each group and then were fixed at a constant pressure of 100 mmHg in 4%

paraformaldehyde. Post fixation, ATAs were cut axially into a top and bottom (basal) half. The top half was flash frozen in O.C.T. Compound and cut into 10 μm cross-sections using a cryotome. Sections were placed on bonded slides and cover slipped using ProLong™ diamond antifade mountant. The bottom half was cut transversely, placed on a bonded slide, and similarly cover slipped for *en face* imaging of the luminal surface. A Leica Sp-8 DIVE Multiphoton was used to image z-stacks of elastic fibers by autofluorescence (excitation: 880 nm, emission: 495–540 nm) and collagen by second harmonic generation imaging (excitation: 880 nm, emission: 420–460 nm). Z-stacks from *en face* samples were trimmed using Image J (NIH) to include only the first layer of elastic fibers (the internal elastic lamina) and a maximum projection was made of the internal elastic lamina region. Holes in the internal elastic lamina, including fenestrations and larger breaks, were quantified by manual thresholding in Image J and determination of hole area using a custom MATLAB code. Hole area was quantified for the three ATAs imaged in each group and results are presented in a combined histogram.

Statistical Analysis

Two ATAs were excluded from the UNT and ELA + PGG groups due to leaks that compromised mechanical testing data and drug treatment efficacy. One ATA was excluded from the parameter fitting for the ELA group because it tore before all six mechanical test protocols could be completed. Statistical analysis was performed in Prism (Graphpad). Mean values are reported with standard deviation error bars. Experimental groups were compared using a one-way ANOVA with Tukey's multiple comparisons for the mechanical testing data. Pair-wise comparisons were also performed since each ATA served as its own control (presented in supplemental data), but the pairwise statistics did not allow comparisons between treatment groups (i.e. ELA to PGG-ELA). $P < 0.05$ was considered significant. Imaging data was compared qualitatively to provide possible explanations for the mechanical changes.

RESULTS

Biaxial Mechanical Behavior

ATAs were subjected to multiple inflation cycles at constant axial stretch and axial stretch cycles at constant pressure to characterize the biaxial mechanical behavior with ELA-induced elastic fiber degradation and PGG treatment. Average pressure-diameter, -axial force, and -compliance behavior for each treatment group at the lowest constant axial stretch ratio tested are shown in Figs. 2a–2c. The lowest axial stretch ratios tested are shown in Fig. 2d. No significant differences in diameter, axial force, or compliance are found between PGG and UNT ATAs at any pressure, suggesting that PGG specifically targets degraded elastic fibers and does not disrupt mechanical behavior of the native mouse ATA. In comparison, ELA ATAs have diameters that are 9–54% larger, axial forces that are reduced by 10–30 mN, and compliance that is increased by 130–280% at low pressures and decreased by 50–90% at high pressures compared to UNT ATAs, demonstrating the mechanical changes in mouse ATA associated with mild elastic fiber degradation.

Comparing the PGG + ELA and ELA + PGG ATAs to the UNT and ELA ATAs, there are differences between preventative and restorative PGG treatment. The PGG + ELA curves are closer to the UNT curves in Figs. 2a and 2c, while the ELA + PGG curves are closer to the ELA curves, indicating that preventative PGG treatment is more effective at ameliorating mechanical changes associated with elastic fiber degradation than restorative PGG treatment. This is supported by the fact that there are significant differences in diameter (Fig. 2a) and compliance (Fig. 2c) between PGG + ELA and UNT at less of the applied pressure values than there are for ELA + PGG compared to UNT. It is important to point out, however, that restorative PGG treatment appears to stabilize the elastic fibers to a degree, as the ELA + PGG diameter and compliance is not significantly different from UNT at some pressures. Tukey's multiple comparison analyses of PGG + ELA vs. ELA + PGG show differences between the two treatments for diameter and compliance measurements at 50 and 75–125 mmHg, respectively (Supp. Table 1).

The differences in pressure-axial force behavior between UNT/PGG and ELA ATAs (Fig. 2b) are mostly the result of the applied axial stretch ratio during testing (Fig. 2d). Due to lengthening of the ATA with ELA treatment and tearing of the tissue when stretched beyond an axial stretch ratio of 1.3–1.4, we could not test the groups under the same axial loading protocols. Lengthening and decreased axial distensibility in response to ELA treatment occurs in dog carotid arteries, human iliac arteries,[10] and mouse ATA[5] and is likely caused by uncrimping of collagen fibers when elastic fibers are degraded.[15] We fitted the HGO constitutive model to our data so that we could extend our comparisons between groups to similar loading conditions.

Pairwise comparisons of the diameter, axial force, and compliance for each ATA at 75 mmHg, near diastolic pressure in the mouse and the range expected

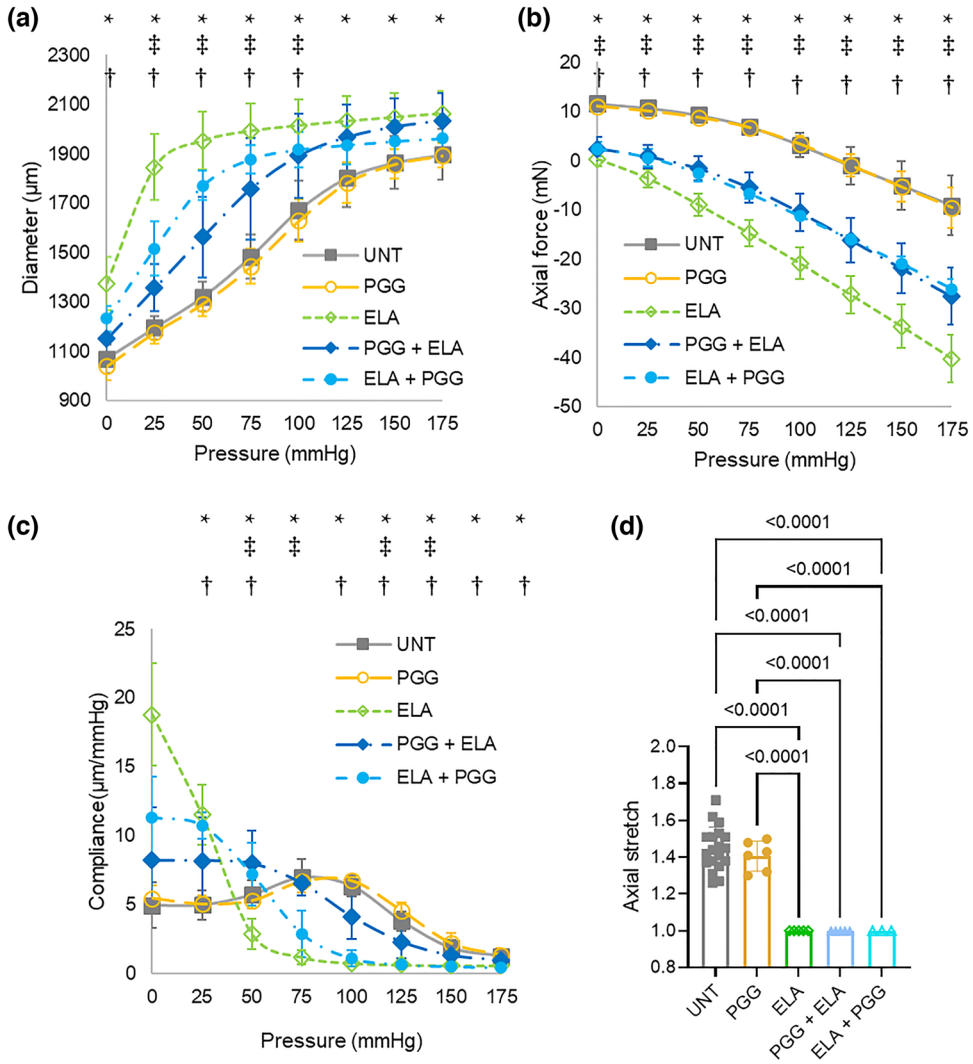

FIGURE 2. Average data from the cyclic pressurization protocol at the lowest constant axial stretch. Diameter-pressure (a), axial force-pressure (b), and compliance-pressure (c) for experimental groups at the given axial stretch values (d). For A – C, comparisons are made to the UNT group using one-way ANOVA with Tukey's posthoc and *P* values < 0.05 are noted by *, ‡, †, for ELA, PGG + ELA, ELA + PGG, respectively. For D, comparisons are made between all groups using one-way ANOVA with Tukey's posthoc and significant P values are shown. No significant differences were found comparing PGG to UNT. *N* = 19 for UNT, *N* = 3–6/group for all others.

to be important for elastic fiber contributions, are presented in Supp. Figure 1.

Unloaded Dimensions

The unloaded length of the ATA was measured before and after drug treatment. The length ratio was unchanged after PGG treatment, but was increased after ELA, PGG + ELA, and ELA + PGG treatment (Fig. 3a). The length increased by 14 ± 10% compared to the original unloaded length in all ELA treated groups with no significant differences between ELA treated groups. Our results suggest that PGG treatment does not prevent ATA lengthening associated with mild elastic fiber degradation. The unloaded diameter of the ATA was increased 6–11% in the ELA groups compared to the PGG treated group (Fig. 3b). Our results suggest that PGG treatment does prevent the unloaded diameter dilation associated with mild elastic fiber fragmentation. The unloaded thickness did not change with drug treatment (Fig. 3c). As there were no significant differences in the unloaded diameters and thicknesses between the PGG, PGG + ELA, and ELA + PGG groups and we did not have unloaded diameters and thicknesses for the UNT group (since every UNT ATA was also used in a drug treatment group), we used the average unloaded diameters and thicknesses for the PGG, PGG + ELA, and ELA + PGG groups as the unloaded dimensions for all UNT ATAs for stretch and stress calculations.

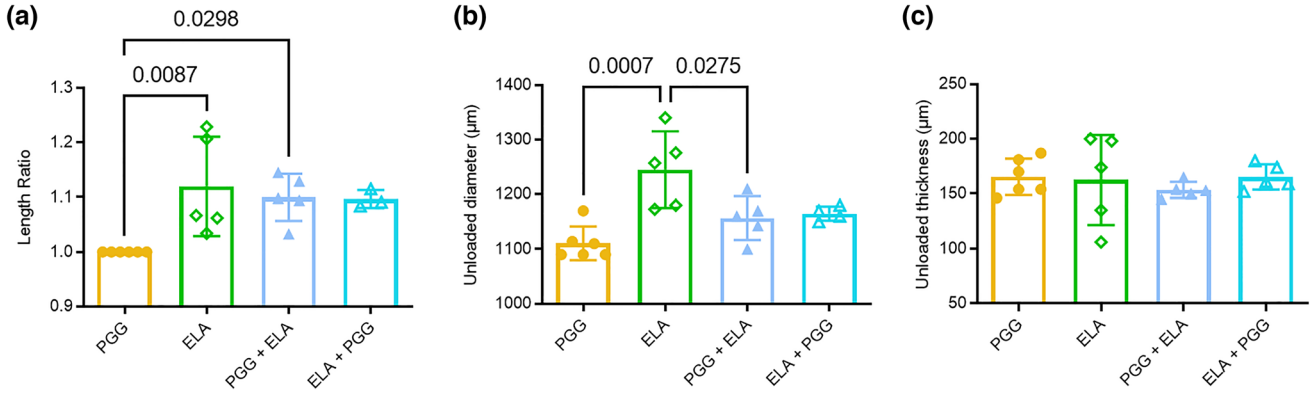

FIGURE 3. Unloaded dimensions for different treatment groups. Unloaded length ratio (after/before treatment) (a), unloaded diameter (b), and unloaded thickness (c) of the ATA for the four treatment groups. Significant *p*-values from one-way ANOVA with Tukey's posthoc are shown. *N* = 3–6/group.

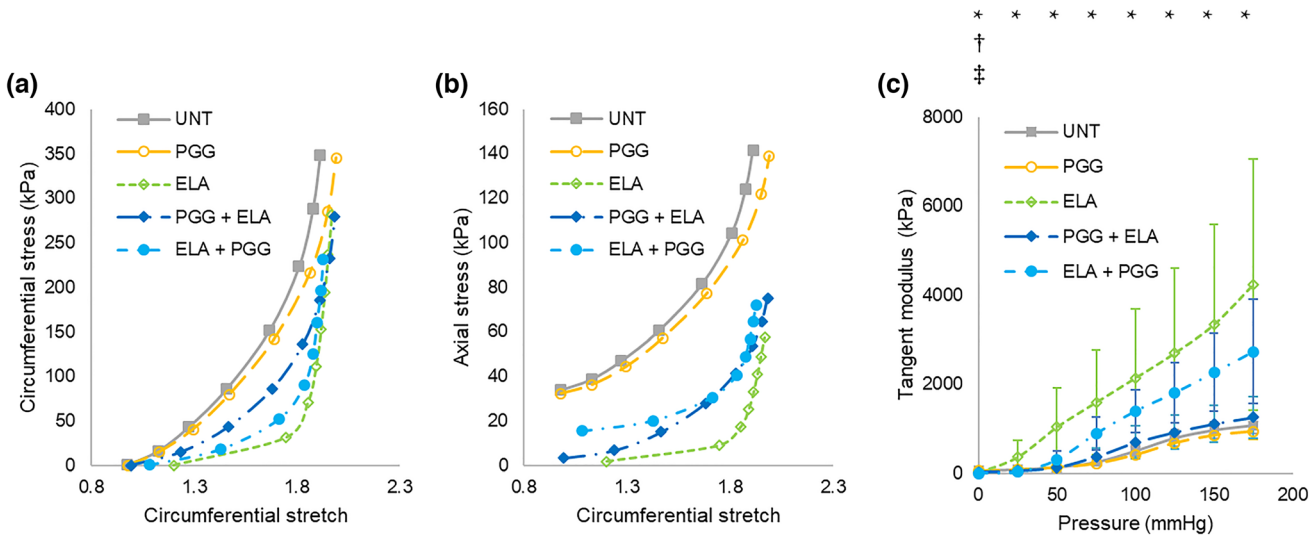

FIGURE 4. Material behavior from the cyclic pressurization protocol at the lowest constant axial stretch. Circumferential stress-circumferential stretch (a), axial stress-circumferential stretch (b), and circumferential tangent modulus-pressure (c) for experimental groups. Error bars are not shown for A and B for clarity and because stress and stretch values varied at each pressure for each ATA. Statistical comparisons are made in C to the UNT group using one-way ANOVA with Tukey's posthoc and *P*-values < 0.05 are noted by *, ‡, †, for ELA, PGG + ELA, ELA + PGG, respectively. No significant differences were found comparing UNT to PGG. *N* = 19 for UNT, *N* = 3–6/group for all others.

For the treatment groups, the individual ATA unloaded dimensions were used.

Stresses and Circumferential Tangent Modulus

The biaxial mechanical test data and unloaded dimensions were used to calculate the circumferential and axial stresses and circumferential tangent modulus for the cyclic inflation protocol at the lowest constant axial stretch (Fig. 4). As each ATA had applied stretches and stresses that depend on the unloaded dimensions, the stretch–stress curves are not quantitatively compared. Qualitatively, Figs. 4a and 4b show the similarities between the UNT and PGG groups, the changes in nonlinearity of the curves with ELA treatment, and the partial recovery of the material behavior with PGG treatment. Additionally, Figs. 4a and 4b highlight that preventative PGG + ELA treatment is more effective than restorative ELA + PGG treatment at returning the material behavior near UNT values, especially in the circumferential direction. The pressure-tangent modulus behavior (Fig. 4c) demonstrates significant stiffening of the ATA at high pressures in the ELA group due to the elastic fiber degradation. Similar to the pressure-diameter and pressure-compliance behavior (Figs. 2a and 2c), the pressure-modulus behavior of the PGG + ELA group is more similar to UNT, while the ELA + PGG group is more similar to ELA. The stress and modulus curves demonstrate that PGG does not change material

behavior of the native mouse ATA and that it partially ameliorates changes due to mild elastic fiber degradation associated with TAA.

Like the pressure-axial force behavior (Fig. 2b), the differences in axial stress behavior (Fig. 4b) are mostly the result are different applied axial stretch ratios (Fig. 2d). However, increased axial stretch would cause an increase in tangent modulus, exaggerating the differences already observed in the ELA group (Fig. 2c). Also, the ELA, PGG + ELA, and ELA + PGG groups are all at the same axial stretch ratio and so the axial stresses can be compared. The axial stresses for the ELA treated groups show that even though we did observe axial lengthening in all groups (Fig. 3a), the axial stress behavior associated with degraded elastic fibers (ELA) is partially returned toward UNT values with both preventative (PGG + ELA) and restorative (ELA + PGG) PGG treatment.

Pairwise comparisons of the circumferential and axial stresses and tangent modulus for each ATA at 75 mmHg are presented in Supp. Fig. 2.

Constitutive Modeling

The HGO constitutive model was fitted to the experimental data to evaluate goodness of fit, to predict contributions of the isotropic and anisotropic components, and to compare groups under consistent loading conditions. Representative fits are shown in Supp. Fig. 3. The model fits the UNT and PGG groups well ($R^2 = 0.84 \pm 0.03$ and 0.88 ± 0.02, respectively) (Fig. 5a). R^2 for the ELA group is only 0.44 ± 0.03, indicating that the effects of elastic fiber degradation are severe enough that the mechanical behavior can no longer be well-described by a commonly used arterial constitutive model. R^2 in the PGG + ELA and ELA + PGG groups is significantly reduced compared to UNT and PGG and significantly increased compared to ELA, but is not significantly different between groups (average $R^2 = 0.66 \pm 0.08$ for both groups). The differences in R^2 with either preventative or restorative PGG treatment compared to ELA indicate that the changes in mechanical behavior associated with elastic fiber degradation are ameliorated enough by PGG that a commonly used arterial constitutive model can better approximate the behavior.

The parameter (c_1) for the isotropic, neo-Hookean term, typically associated with elastic fibers in the arterial wall,[18] is not significantly different between UNT and PGG groups (average $c_1 = 21.4 \pm 3.0$ kPa for both groups), but is significantly different between UNT/PGG and all ELA treated groups (Fig. 5b). The ELA treated groups are not significantly different from each other and the average $c_1 = 0.21 \pm 0.38$ kPa, or essentially zero, indicating no contribution from the isotropic, neo-Hookean component. The parameters associated with the anisotropic, exponential fibers, typically associated with collagen fibers in the arterial wall,[18] are difficult to compare directly (Figs. 5c–5f). However, the ratio of $\frac{c_2}{c_3}$ gives an estimate of the relative nonlinearity of the behavior, with a lower ratio indicating more nonlinear behavior. The ratio (Fig. 5f) is 77% higher in UNT compared to ELA groups, with no significant differences between UNT and all other groups, indicating the nonlinear behavior induced by mild elastic fiber degradation and the partial amelioration of this behavior with PGG treatment. The angle, α, represents the angle of the fibers in the unloaded configuration with respect to the circumferential direction. The angle is increased from 38° in UNT to 44° in PGG + ELA (Fig. 5e), indicating that the PGG + ELA treatment may affect ATA anisotropy. Pairwise comparisons of the fitted parameters for each ATA are presented in Supp. Fig. 4.

To illustrate changes in nonlinearity and anisotropy, we applied a theoretical equibiaxial stretch of 1.0–2.0 to representative ATAs with parameters near the mean of each group and calculated the stored strain energy, stresses, and incremental moduli as a function of stretch (Fig. 6). All curves show the similarity of the UNT and PGG behavior, the increased nonlinearity of the ELA behavior and the partial rescue of the nonlinearity with PGG treatment. In particular, the amount of stored strain energy in the ELA group is low in the physiologic stretch range of 1.4–1.8 (Fig. 6b), indicating the lack of aortic elasticity with fragmented elastic fibers. The UNT, PGG, and ELA groups are more anisotropic, with increased circumferential moduli compared to axial (Figs. 6e and 6f), while the PGG + ELA and ELA + PGG groups are more isotropic, consistent with the variation in fitted fiber angles (Fig. 5e). The PGG + ELA and ELA + PGG groups are more similar to UNT in the circumferential direction, but to ELA in the axial direction (Figs. 6b–6f), indicating that the treatment is more effective at ameliorating circumferential changes than axial, as supported by the changes in length ratio (Fig. 3a) and unloaded diameter (Fig. 3b). Note that the experimental axial stretch ratios for the ELA, PGG + ELA, and ELA + PGG groups were only 1.0–1.2, so caution must be taken in interpreting these curves at the higher axial stretch values.

Extracellular Matrix Structure

Cross-sections of the treated ATAs were imaged to qualitatively compare changes in the extracellular matrix structure (Fig. 7) that may explain differences

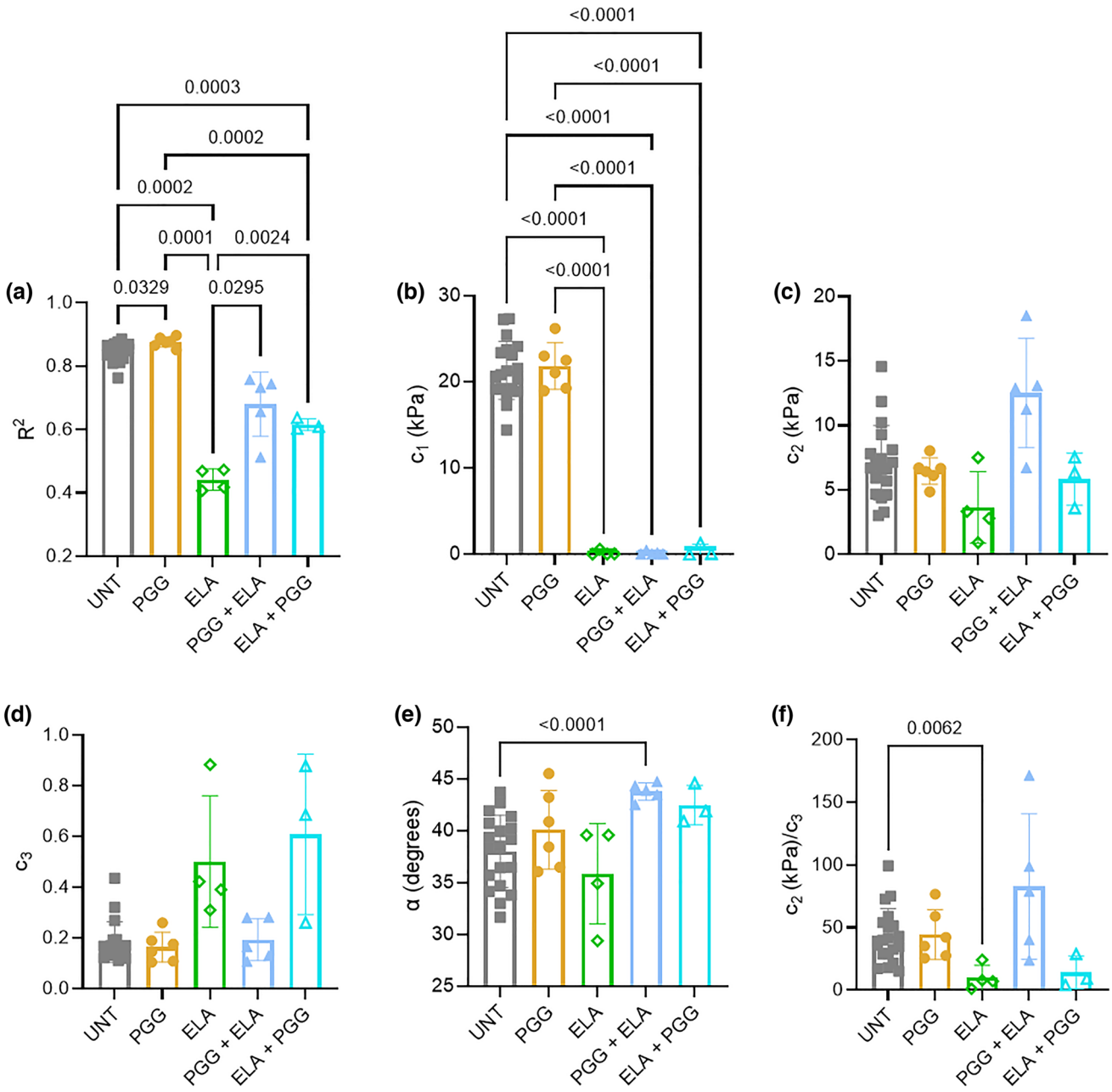

FIGURE 5. Fitting of the HGO constitutive model. Goodness of fit (R^2) (a), isotropic constant (c_1) (b), anisotropic constants (c_2, c_3), fiber angle (α), and ratio of anisotropic constants (c_2/c_3) are shown. Significant p-values from one-way ANOVA with Tukey's posthoc are shown. N = 19 for UNT, N = 3–6/group for all others.

in mechanical behavior. In the UNT group, nearly straight layers of elastic fibers (elastic lamina) are observed in the medial (middle) layer of the wall, with wavy collagen fibers visible in the adventitial (outer) layer of the wall (Fig. 7a). In the ELA and ELA + PGG groups, there appears to be dissociation of the elastic and collagen fiber layers at the medial-adventitial border (Figs. 7c and 7e). There is buckling of these regions which is not expected, since the ATAs were fixed at 100 mmHg. The buckling may play a role in the highly nonlinear circumferential mechanical behavior observed in the ELA and to some extent the ELA + PGG groups. The dissociation and buckling is less severe in the ELA + PGG group compared to ELA, suggesting that restorative PGG treatment can partially prevent this behavior. The dissociation and buckling is not apparent in the PGG + ELA group (Fig. 7d), suggesting that preventative PGG treatment can block this behavior.

(a)

Parameters for representative samples.					
Group	R^2	c_1 (kPa)	c_2 (kPa)	c_3	α (°)
UNT	0.88	20.0	6.61	0.155	34.2
PGG	0.87	23.0	6.12	0.145	42.2
ELA	0.42	0	3.32	0.423	34.9
PGG + ELA	0.74	0	13.10	0.166	43.9
ELA + PGG	0.64	0.004	7.55	0.261	44.6

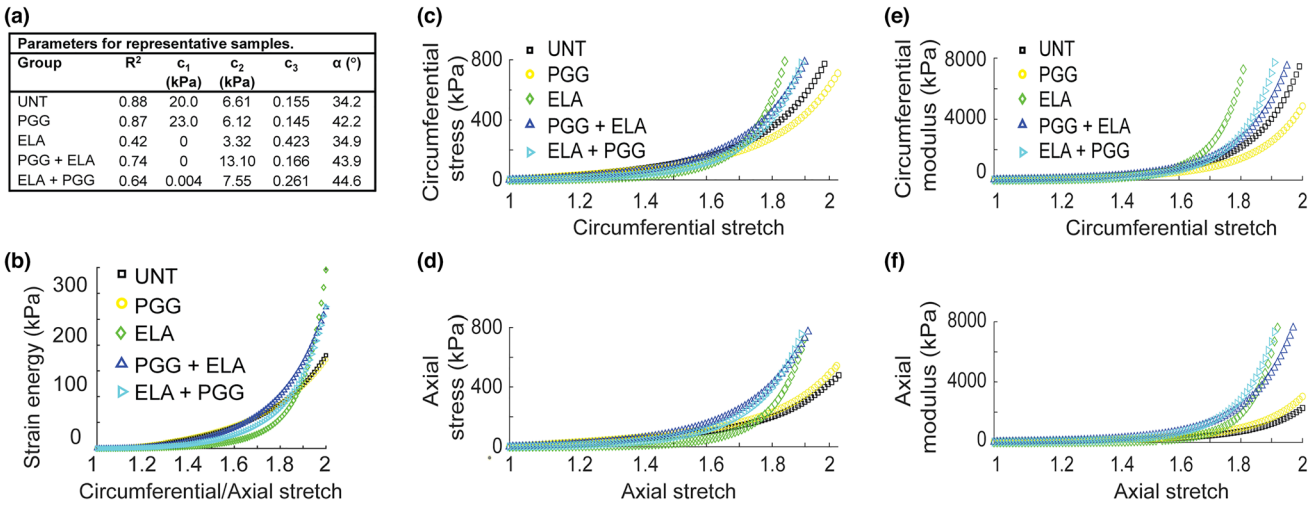

FIGURE 6. Comparison of representative samples under identical loading protocols. Equibiaxial tests from 1.0 to 2.0 stretch were simulated using fitted parameters (a) for representative samples in each group. Stored strain energy (b), circumferential (c), and axial (d) stress and circumferential (e) and axial (f) incremental moduli are shown as a function of stretch.

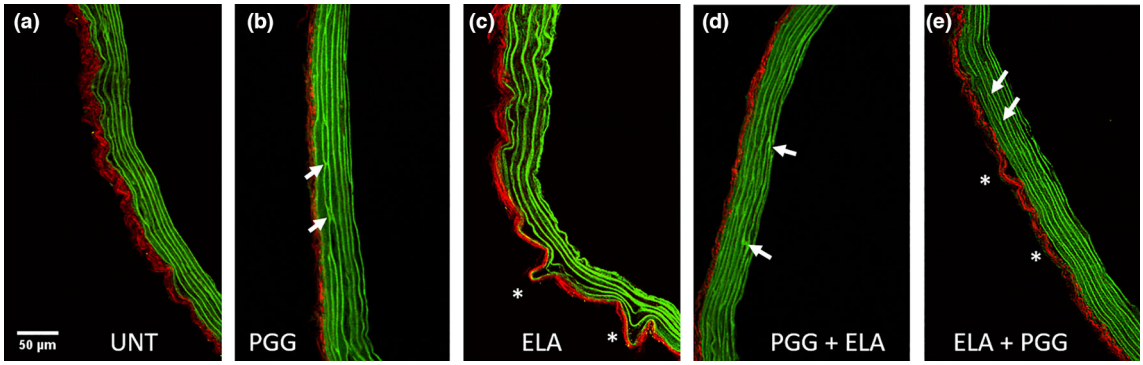

FIGURE 7. Multiphoton images of ATA cross-sections: UNT (a), PGG (b), ELA (c), PGG + ELA (d), and ELA + PGG (e). Elastin is shown in green, collagen in red. Arrows point to laminae adhesions and asterisks identify separation and buckling of the collagenous adventitia. Scale bar = 50 μm.

While all elastic lamina have regions where they appear to adhere to or merge with other layers, there appear to be more elastic lamina adhesions in the PGG treated groups (Figs. 7b, 7d and 7e) compared to others. While the elastic lamina adhesions do not appear to affect the mechanical behavior of the PGG group, they may play a role in preventing mechanical changes associated with elastic fiber fragmentation in the PGG + ELA and ELA + PGG groups. PGG binds hydrophobic regions of extracellular matrix proteins,[29] including elastin and collagen, which may explain the physical characteristics of PGG preventing elastic and collagen fiber dissociation and facilitating elastic lamina adhesions.

The *en face* images, which show the internal elastic lamina, also have differences specific to each treatment group (Fig. 8). ATAs treated with ELA show large gaps or holes in the elastic fiber structure (Figs. 8c, 8d, and e) that are different from fenestrations, which are small round holes present in the internal elastic lamina. The structural gaps in the internal elastic lamina are quantified by histograms that display the area of the holes. The histograms all have a main peak at 10 μm^2, near the expected area of the fenestrations,[26] but the ELA treated groups have additional holes with larger areas (60–170 μm^2). No artifacts specific to PGG treatment can be seen in the *en face* images.

DISCUSSION

Previous work focused on the use of PGG to prevent elastic fiber degradation and dilation in animal models of AAA.[9,28,32,35] Here, we present an *in vitro* mouse model of ATA dilation due to enzymatic degradation of the elastic fibers and amelioration of the associated changes in mechanical behavior by PGG treatment. We found that preventative treatment with

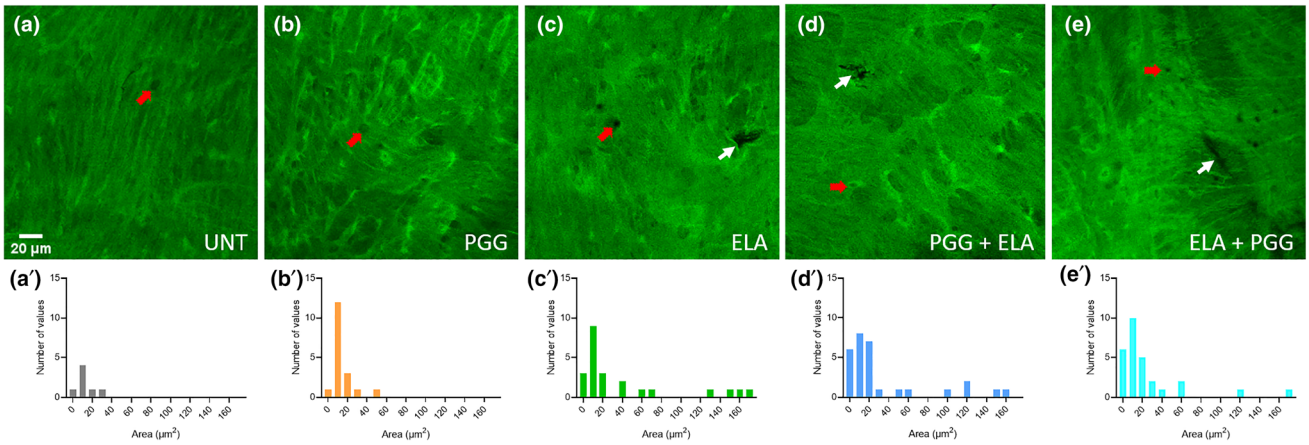

FIGURE 8. Multiphoton images of ATA en face sections with a maximum projection of the internal elastic lamina: UNT (a), PGG (b), ELA (c), PGG + ELA (d), and ELA + PGG (e). Elastin is shown in green. Red arrows point to fenestrations in the laminae and white arrows point to larger breaks. Scale bar = 20 μm. Histograms of the measured areas of each IEL hole (fenestration or larger break) are shown below each image (a′–e′) (N = 3 images quantified/group).

PGG + ELA, before enzymatic digestion with elastase, best matched our UNT ATAs for most mechanical parameters. However, restorative treatment with ELA + PGG, after enzymatic digestion with elastase, prevented some changes, including the diameter increase in the unloaded condition and the large decrease in goodness of fit for a traditional arterial strain energy function. Our results provide motivation for further investigating the ability of PGG to prevent or restore mechanical changes in TAAs associated with elastic fiber fragmentation.

Relevance of In Vitro Studies

Other groups investigated *in vivo* PGG treatment for different animal models of AAA. Isenburg *et al.*[22] showed that periadventitial 0.3% PGG treatment prevented and reversed elastic fiber degradation and diameter dilation in a rat $CaCl_2$ AAA model. Schack *et al.*[31] showed that elastic fiber integrity was preserved and diameter dilation was prevented in a rat elastase AAA model, but only when 0.6 mg/mL PGG was delivered for 15 min intraluminally and not through a drug-eluting stent. Delivery of PGG encapsulated in nanoparticles coated with an antibody to degraded elastin reversed elastic fiber degradation, diameter dilation, and decreases in circumferential strain in mouse elastase[9] and $LDLR^{-/-}$ Ang II[35] AAA models. However, Anderson *et al.*[2] found that periadventitial 0.3% PGG treatment did not prevent diameter dilation in elastase or $CaCl_2$ mouse AAA models, but did partially restore circumferential strain. In these *in vivo* studies, elastic fiber stabilization and additional effects of PGG, including reduced matrix metalloproteinase production, macrophage infiltration, and/or TGF-β1 activity,[9,22,35] may be differentially affected by the aneurysm model and PGG delivery mode. Controlled *in vitro* studies are needed to isolate effects of PGG on specific factors that contribute to aneurysm progression, such as degraded elastic fibers.

Importance of TAA-Specific Investigations

We previously investigated *in vitro* preventative PGG treatment for mouse carotid arteries after elastase exposure.[30] There were two main differences between the results for our carotid and ATA studies: (1) PGG did not prevent or reverse the lengthening observed with ELA treatment in the ATA (Fig. 3a) and (2) PGG did not affect the pressure-diameter (Fig. 2a) or -compliance (Fig. 2c) behavior compared to UNT in the ATA. There are differences in the amounts of elastin and collagen in the wall[13] and the *in vivo* stretch[34] of ATAs compared to carotids that may explain these results. We also used a milder treatment protocol for the elastase digestion and PGG protection for the ATA studies, with application only to the lumen of the artery, rather than in the surrounding fluid. As PGG binds to collagen, as well as elastin,[29] the intraluminal delivery, different from previous whole artery submersion, may have prevented the stiffening that we previously observed with PGG treated carotids. PGG is approximately 1 kDa and solute flux through the ATA wall is expected under our experimental conditions,[8] however PGG would be less concentrated at the adventitial (outer) surface compared to the intimal (inner) surface after 7 min of luminal exposure.

Patnaik *et al.*[29] found that restorative PGG treatment was effective at reversing some of the mechanical effects associated with ELA treatment in *in vitro* studies of the pig abdominal aorta. However, there are

reduced amounts of elastin in the abdominal aorta compared to the ATA[13] and the association of genetic mutations in elastic fiber genes with aneurysm formation is specific to the thoracic aorta.[12,24] Hence, TAA-specific models are needed to evaluate the potential of PGG as a treatment option. Although ELA treatment is a crude model of TAA, it has been informative in comparing aortic mechanical changes associated with genetic models of TAA[5] and allows well-controlled *in vitro* conditions to evaluate PGG effects.

Preventative vs. Restorative PGG Treatment

Our results for an *in vitro* mouse elastase TAA model indicate that preventative PGG treatment is more effective than restorative PGG treatment in maintaining mechanical behavior near UNT and different from ELA (Figs. 2, 5). As there are no live cells in our study to repair or regenerate extracellular matrix after ELA + PGG treatment, we believe that the restorative behavior is caused by preventing additional damage that occurs after treatment. We speculate that in our protocol, ELA treatment at the minimum axial stretch and 100 mmHg degrades some elastic fibers and connections between extracellular matrix fibers and that subsequent PGG treatment prevents additional degradation that occurs over time or with repeated mechanical testing cycles. This is supported by the differences in collagen and elastic fiber buckling and elastic laminae adhesions in the cross-sectional images in Fig. 7. These results suggest that mechanical stabilization of extracellular matrix alone, without the additional expected beneficial effects of PGG *in vivo*,[9,22,35] may be effective at slowing or preventing TAA dilation. As TAAs can be linked to genetic mutations that may be diagnosed by family history before significant aortic dilation occurs,[12] preventative or early restorative PGG treatment to stabilize elastic fibers may be a viable clinical care strategy.

PGG Effects on Biaxial Mechanical Behavior

In vivo, the ATA is deformed biaxially, with significant circumferential strain due to blood pressure and axial strain due to motion of the heart.[4] In the current study, we investigated ATA biaxial mechanical behavior, rather than circumferential behavior only as we did for carotids,[30] which is critical to mimic the *in vivo* ATA environment. Biaxial mechanical data at the lowest constant axial stretch (Fig. 4) and simulated equibiaxial stretch data using material parameters from representative ATAs (Fig. 6) demonstrate that PGG treatment is more effective at maintaining mechanical behavior near UNT and different from ELA in the circumferential compared to the axial direction. Restoration of the circumferential mechanical behavior with PGG treatment is consistent with previous studies on mouse carotids,[30] mouse abdominal aorta,[35] and pig abdominal aorta.[29] To our knowledge, Patnaik *et al.*[29] is the only group that performed biaxial mechanical testing in an aneurysm model with PGG treatment and they also found PGG to be more effective at restoring circumferential, rather than axial, mechanical behavior. Our interpretation of the axial mechanical behavior is hampered by the limited axial stretch that we could apply experimentally to the ELA treated groups. However, the changes in axial mechanical behavior should be considered and further investigated as they may contribute to arterial tortuosity that is a known characteristic and possible risk factor in some genetic TAAs.[27]

Limitations

Our mechanical characterization was limited by assuming the unloaded dimensions of the UNT ATAs, rather than measuring these values directly, and by the reduced range of experimental axial stretch values possible in the ELA treated groups. Our study used an *in vitro* TAA model and PGG delivery, rather than a more clinically relevant *in vivo* model. Possible *in vivo* PGG delivery methods include nanoparticles targeted to degraded elastin,[9,35] drug-eluting stents,[31] and weeping balloons.[32] *In vivo* chemically-induced TAA models in mice include elastase application to the thoracic aorta[23] and various combinations of β-aminoproprionitrile (BAPN), which inhibits elastin and collagen crosslinking, with AngII, which induces hypertension and an inflammatory response.[37] Genetic mouse models of TAA are also available[12] that do not require chemical interventions and may more closely represent the human disease process. Our *in vitro* studies focused on passive mechanical and structural changes in the ATA associated with elastic fiber degradation and restoration or prevention by PGG treatment. Hence, we did not take advantage of additional beneficial aspects of PGG treatment on viable aortic wall cells that have been previously observed, such as reduced matrix metalloproteinase production, macrophage infiltration, and/or TGF-β1 activity.[9,22,35] As TAA and AAA have known differences in causes, progression, and clinical outcomes that have been linked to these pathways, additional *in vivo* studies to evaluate these effects are needed.

CONCLUSIONS AND FUTURE STUDIES

PGG efficacy in ameliorating dilation and mechanical changes associated with elastic fiber degradation and aneurysms depends on the artery investigated,

aneurysm model, PGG delivery method, and direction of mechanical loading. Our study on ATA biaxial mechanical behavior and wall structure with *in vitro* intraluminal delivery of PGG in a mouse elastase model of TAA is an important addition to the body of work investigating the efficacy of PGG for aneurysm treatment. Future work should include *in vivo* PGG delivery methods to investigate its efficacy in preventing and restoring aortic dilation associated with elastic fiber degradation and other mechanisms of aneurysm progression in mouse models of genetic TAA.

SUPPLEMENTARY INFORMATION

The online version contains supplementary material available at https://doi.org/10.1007/s10439-022-03093-x.

ACKNOWLEDGMENTS

This work was partially supported by the American Heart Association (19TPA-34910047 to JW) and the Marfan Foundation (Faculty Grant Program to JW). BC and MV were supported by the BioMedRAP and WUSEF programs at Washington University, respectively.

CONFLICT OF INTEREST

NRV has shares in Elastrin Therapeutics Inc., which has licensed elastin-targeted nanoparticle therapy from Clemson University.

REFERENCES

[1]Amin, M., A. G. Kunkel, V. P. Le, and J. E. Wagenseil. Effect of storage duration on the mechanical behavior of mouse carotid artery. *J Biomech. Eng*. 133:071007, 2011.

[2]Anderson, J. L., E. E. Niedert, S. S. Patnaik, R. Tang, R. L. Holloway, V. Osteguin, E. A. Finol, and C. J. Goergen. Animal model dependent response to pentagalloyl glucose in murine abdominal aortic injury. *J. Clin. Med*. 10:219, 2021.

[3]Baek, S., R. L. Gleason, K. R. Rajagopal, and J. D. Humphrey. Theory of small on large: potential utility in computations of fluid-solid interactions in arteries. *Comput. Methods Appl. Mech. Eng*. 196:3070–3078, 2007.

[4]Bell, V., W. A. Mitchell, S. Sigurethsson, J. J. Westenberg, J. D. Gotal, A. A. Torjesen, T. Aspelund, L. J. Launer, A. de Roos, V. Gudnason, T. B. Harris, and G. F. Mitchell. Longitudinal and circumferential strain of the proximal aorta. *J. Am. Heart Assoc*. 3:e001536, 2014.

[5]Bellini, C., M. R. Bersi, A. W. Caulk, J. Ferruzzi, D. M. Milewicz, F. Ramirez, D. B. Rifkin, G. Tellides, H. Yanagisawa, and J. D. Humphrey. Comparison of 10 murine models reveals a distinct biomechanical phenotype in thoracic aortic aneurysms. *J. R. Soc. Interface*. 14:20161036, 2017.

[6]De Cario, R., M. Giannini, G. Cassioli, A. Kura, A. M. Gori, R. Marcucci, S. Nistri, G. Pepe, B. Giusti, and E. Sticchi. Tracking an elusive killer: state of the art of molecular-genetic knowledge and laboratory role in diagnosis and risk stratification of thoracic aortic aneurysm and dissection. *Diagnostics (Basel)*. 12:1785, 2022.

[7]Cocciolone, A. J., J. Z. Hawes, M. C. Staiculescu, E. O. Johnson, M. Murshed, and J. E. Wagenseil. Elastin, arterial mechanics, and cardiovascular disease. *Am. J. Physiol. Heart Circ. Physiol*. 315:H189–H205, 2018.

[8]Cocciolone, A. J., E. Johnson, J. Y. Shao, and J. E. Wagenseil. Elastic fiber fragmentation increases transmural hydraulic conductance and solute transport in mouse arteries. *J. Biomech. Eng*. 2018. https://doi.org/10.1115/1.4042173.

[9]Dhital, S., and N. R. Vyavahare. Nanoparticle-based targeted delivery of pentagalloyl glucose reverses elastase-induced abdominal aortic aneurysm and restores aorta to the healthy state in mice. *PLoS ONE*. 15:e0227165, 2020.

[10]Dobrin, P. B., T. H. Schwarcz, and R. Mrkvicka. Longitudinal retractive force in pressurized dog and human arteries. *J. Surg. Res*. 48:116–120, 1990.

[11]Duca, L., S. Blaise, B. Romier, M. Laffargue, S. Gayral, H. El Btaouri, C. Kawecki, A. Guillot, L. Martiny, L. Debelle, and P. Maurice. Matrix ageing and vascular impacts: focus on elastin fragmentation. *Cardiovasc Res*. 110:298–308, 2016.

[12]Faggion Vinholo, T., A. J. Brownstein, B. A. Ziganshin, M. A. Zafar, H. Kuivaniemi, S. C. Body, A. E. Bale, and J. A. Elefteriades. Genes associated with thoracic aortic aneurysm and dissection: 2019 update and clinical implications. *Aorta (Stamford)*. 7:99–107, 2019.

[13]Faury, G., M. Pezet, R. H. Knutsen, W. A. Boyle, S. P. Heximer, S. E. McLean, R. K. Minkes, K. J. Blumer, A. Kovacs, D. P. Kelly, D. Y. Li, B. Starcher, and R. P. Mecham. Developmental adaptation of the mouse cardiovascular system to elastin haploinsufficiency. *J. Clin. Invest*. 112:1419–1428, 2003.

[14]Ferruzzi, J., D. A. Vorp, and J. D. Humphrey. On constitutive descriptors of the biaxial mechanical behaviour of human abdominal aorta and aneurysms. *J. R. Soc. Interface*. 8:435–450, 2011.

[15]Fonck, E., G. Prod'hom, S. Roy, L. Augsburger, D. A. Rufenacht, and N. Stergiopulos. Effect of elastin degradation on carotid wall mechanics as assessed by a constituent-based biomechanical model. *Am. J. Physiol. Heart Circ. Physiol*. 292:H2754–H2763, 2007.

[16]Guang, Y., A. J. Cocciolone, C. L. Crandall, B. B. Johnston, L. A. Setton, and J. E. Wagenseil. A multiphasic model for determination of water and solute transport across the arterial wall: effects of elastic fiber defects. *Arch. Appl. Mech*. 92:447–459, 2022.

[17]Hawes, J. Z., A. Cocciolone, A. H. Cui, D. B. Griffin, M. C. Staiculescu, R. P. Mecham, and J. E. Wagenseil. Elastin haploinsufficiency in mice has divergent effects on arterial remodeling with aging depending on sex. *Am. J. Physiol. Heart Circ. Physiol*. 319:H1398, 2020.

[18]Holzapfel, G. A., T. C. Gasser, and R. W. Ogden. A new constitutive framework for arterial wall mechanics and a comparative study of material models. *J. Elastic*. 61:1–48, 2000.

[19]Humphrey, J. D. Cardiovascular Solid Mechanics. New York: Springer-Verlag, p. 757, 2002.
[20]Ince, H., and C. A. Nienaber. Etiology, pathogenesis and management of thoracic aortic aneurysm. *Nat. Clin. Pract. Cardiovasc. Med.* 4:418–427, 2007.
[21]Isenburg, J. C., N. V. Karamchandani, D. T. Simionescu, and N. R. Vyavahare. Structural requirements for stabilization of vascular elastin by polyphenolic tannins. *Biomaterials*. 27:3645–3651, 2006.
[22]Isenburg, J. C., D. T. Simionescu, B. C. Starcher, and N. R. Vyavahare. Elastin stabilization for treatment of abdominal aortic aneurysms. *Circulation*. 115:1729–1737, 2007.
[23]Johnston, W. F., M. Salmon, N. H. Pope, A. Meher, G. Su, M. L. Stone, G. Lu, G. K. Owens, G. R. Upchurch Jr., and G. Ailawadi. Inhibition of interleukin-1beta decreases aneurysm formation and progression in a novel model of thoracic aortic aneurysms. *Circulation*. 130:S51–S59, 2014.
[24]Karimi, A., and D. M. Milewicz. Structure of the elastin-contractile units in the thoracic aorta and how genes that cause thoracic aortic aneurysms and dissections disrupt this structure. *Can. J. Cardiol.* 32:26–34, 2016.
[25]Le, V. P., J. K. Cheng, J. Kim, M. C. Staiculescu, S. W. Ficker, S. C. Sheth, S. A. Bhayani, R. P. Mecham, H. Yanagisawa, and J. E. Wagenseil. Mechanical factors direct mouse aortic remodelling during early maturation. *J. R. Soc. Interface*. 12:20141350, 2015.
[26]Lopez-Guimet, J., J. Andilla, P. Loza-Alvarez, and G. Egea. High-resolution morphological approach to analyse elastic laminae injuries of the ascending aorta in a murine model of Marfan syndrome. *Sci. Rep.* 7:1505, 2017.
[27]Morris, S. A. Arterial tortuosity in genetic arteriopathies. *Curr. Opin. Cardiol.* 30:587–593, 2015.
[28]Nosoudi, N., A. Chowdhury, S. Siclari, V. Parasaram, S. Karamched, and N. Vyavahare. Systemic delivery of nanoparticles loaded with pentagalloyl glucose protects elastic lamina and prevents abdominal aortic aneurysm in rats. *J. Cardiovasc. Transl. Res.* 9:445–455, 2016.
[29]Patnaik, S. S., S. Piskin, N. R. Pillalamarri, G. Romero, G. P. Escobar, E. Sprague, and E. A. Finol. Biomechanical restoration potential of pentagalloyl glucose after arterial extracellular matrix degeneration. *Bioengineering (Basel)*. 6:58, 2019.
[30]Pavey, S. N., A. J. Cocciolone, A. G. Marty, H. N. Ismail, J. Z. Hawes, and J. E. Wagenseil. Pentagalloyl glucose (PGG) partially prevents arterial mechanical changes due to elastin degradation. *Exp. Mech.* 61:41–51, 2021.
[31]Schack, A. S., J. Stubbe, L. B. Steffensen, H. Mahmoud, M. S. Laursen, and J. S. Lindholt. Intraluminal infusion of penta-galloyl glucose reduces abdominal aortic aneurysm development in the elastase rat model. *PLoS ONE*. 15:e0234409, 2020.
[32]Simionescu, D., M. Casco, J. Turner, N. Rierson, J. Yue, and K. Ning. Chemical stabilization of the extracellular matrix attenuates growth of experimentally induced abdominal aorta aneurysms in a large animal model. *JVS Vasc Sci*. 1:69–80, 2020.
[33]Wagenseil, J. E., and R. P. Mecham. Vascular extracellular matrix and arterial mechanics. *Physiol. Rev.* 89:957–989, 2009.
[34]Wagenseil, J. E., N. L. Nerurkar, R. H. Knutsen, R. J. Okamoto, D. Y. Li, and R. P. Mecham. Effects of elastin haploinsufficiency on the mechanical behavior of mouse arteries. *Am. J. Physiol. Heart Circ. Physiol.* 289:H1209–H1217, 2005.
[35]Wang, X., V. Parasaram, S. Dhital, N. Nosoudi, S. Hasanain, B. A. Lane, S. M. Lessner, J. F. Eberth, and N. R. Vyavahare. Systemic delivery of targeted nanotherapeutic reverses angiotensin II-induced abdominal aortic aneurysms in mice. *Sci Rep.* 11:8584, 2021.
[36]Winkler, R. H. The effect of halides (NaCl and NaI) on in vitro pancreatic elastase activity. *Connect. Tissue Res.* 6:89–92, 1978.
[37]Zheng, H. Q., J. B. Rong, F. M. Ye, Y. C. Xu, H. S. Lu, and J. A. Wang. Induction of thoracic aortic dissection: a mini-review of beta-aminopropionitrile-related mouse models. *J. Zhejiang Univ. Sci. B*. 21:603–610, 2020.